Progress in Medical Devices
ISSN: 2957-5478

Zentime

Research Article https://doi.org/10.61189/941872mmikqi

Transformer network–based disease subtyping from multidimensional lesion-layer features

Linrong Yuan*, Yutong Xie*, Danhong Li*, Jianghui Li, Miao Yu, Siqi Wang, Yu Wang, He Ren

Faculty of Medical Instrumentation, Shanghai University of Medicine and Health Sciences, Shanghai 201318, China.
*The authors contribute equally.

Corresponding author: He Ren.

Declaration of conflict of interest: None.

Received July 26, 2025; Accepted September 10, 2025; Published September 30, 2025

Highlights

- A total of 289 patient CT datasets were analyzed, and 15 optimal radiomic features were identified using ANOVA, correlation analysis, and random forest ranking, ensuring high discriminative power and clinical interpretability.
- The proposed model demonstrated excellent performance (Accuracy: 0.98, Area Under the Curve: 0.99) in training set, demonstrating robust learning capacity and the ability to distinguish lesion subtypes from multidimensional radiomic features.
- By leveraging serialized radiomic trends rather than isolated feature analysis, this study provides a new paradigm for early screening and personalized diagnosis of lung adenocarcinoma.

Abstract

Objective: To develop and validate a Transformer-based radiomics model for classifying lung adenocarcinoma subtypes from computed tomography imaging data. **Methods:** We retrospectively collected 289 computed tomography images of lung adenocarcinoma, including adenocarcinoma in situ, minimally invasive adenocarcinoma, and invasive adenocarcinoma. Correlation-based feature analysis was employed and identified 15 optimal radiomic features. A Transformer-based classification model incorporating multi-head attention and position-wise feed-forward Networks was subsequently constructed. **Results:** The proposed model achieved a training accuracy of 0.98, test accuracy of 0.914, training recall of 0.942, test recall of 0.874, training F1-score of 0.940, test F1-score of 0.871, training area under the curve of 0.99, and test area under the curve of 0.88. **Conclusion:** This Transformer-based radiomics model effectively classifies lung adenocarcinoma subtypes, aiding early screening, diagnosis, and personalized treatment strategies to improve patient prognosis.

Keywords: Computed tomography, lung adenocarcinoma subtype analysis, radiomic characteristics, deep learning, transformer network model

Introduction

Cancer remains one of the most prevalent malignancies worldwide, with lung cancer exhibiting the highest incidence and mortality rates in China, showing an upward trend over recent decades [1-4]. Lung adenocarcinoma is the predominant histological type of lung cancer. According to the World Health Organization pathological classification, lung adenocarcinoma is categorized into pre-invasive lesions [e.g., atypical adenomatous hyperplasia, adenocarcinoma in situ (AIS)], minimally invasive adenocarcinoma (MIA), and invasive adenocarcinoma (IAC) [5-8].

Lung adenocarcinoma typically manifests as pulmonary nodules on CT. With continuous advancements in CT technology and deep learning, the screening and detection of pulmonary nodules have rapidly increased [9-12]. Deep learning algorithms enable precise medical image segmentation and feature extraction. Recent studies have shown that Transformer-based and Convolutional Neural Network models significantly improve the accuracy of semantic segmentation and predictive classification in medical imaging [13-15]. Jing and

Address correspondence to: He Ren, Faculty of Medical Instrumentation, Shanghai University of Medicine and Health Sciences; No. 279, Zhouzhu Highway, Pudong New Area, Shanghai 201318, China. Tel: +86-18817581363. E-mail: renh@sumhs.edu.cn.

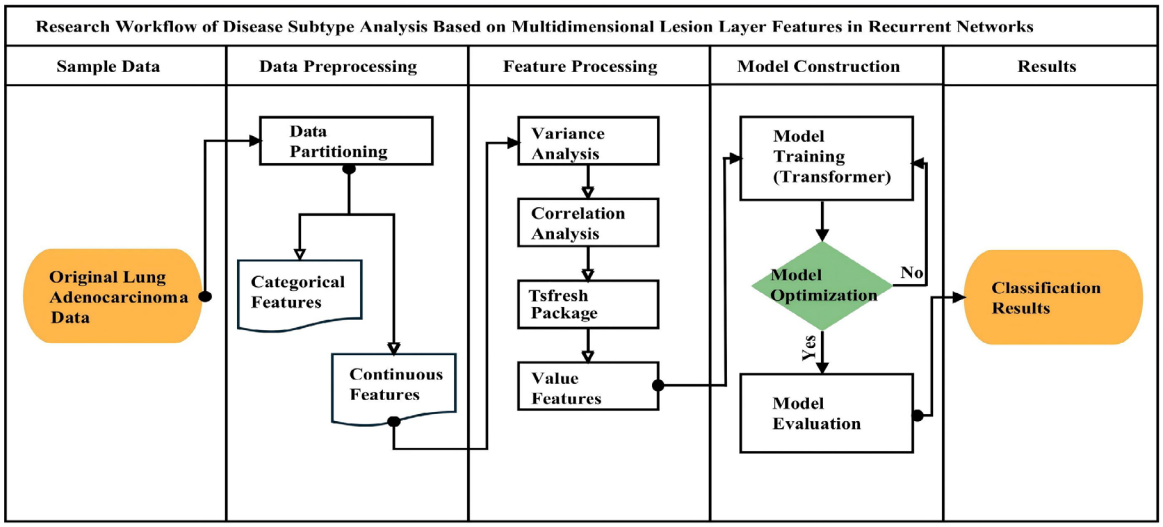

Figure 1. Flowchart of the proposed lung adenocarcinoma subtype classification framework.

Table 1. Baseline characteristics of the included patients

Parameters/Features	Contents
CT equipment	United Imaging 760 CT; Siemens SOMATOM Emotion 16 CT
Scanning parameters	Tube current: 42-126 mA/34-123 mA; Tube voltage: 120-130 kV; Slice thickness: 1 mm; Matrix: 512×512
Reconstruction algorithm	Standard reconstruction algorithm
Radiation dose	Conventional low-dose chest CT scans (42-126 mA; 34-123 mA)
Sex	113 males (39.1%); 176 females (60.9%)
Age	40-75 years (mean 56.3±9.2 years)
Smoking history	85 smokers (29.4%); 204 nonsmokers (70.6%)
Pathological classification	AIS: 50 cases (17.3%); MIA: 172 cases (59.5%); IAC: 67 cases (23.2%)

Note: CT, computed tomography; AIS, adenocarcinoma in situ; MIA, minimally invasive adenocarcinoma; IAC, invasive adenocarcinoma.

Hussein et al. analyzed CT images of pulmonary nodules using specialized software and showed that radiological and imaging characteristics can assist clinicians in differentiating disease subtypes, thereby enhancing model accuracy [16, 17] .

In this study, we adopted feature analysis, machine learning, and recurrent neural networks (**Figure 1**). By integrating imaging and radiological features from a lung adenocarcinoma dataset, we applied appropriate feature-selection algorithms to identify predictive features for disease subtype classification. Using targeted radiomics feature sequences, we developed a classification model that combined radiomics and Transformer networks. The integrated approach facilitated early screening and diagnosis of lung adenocarcinoma and supported clinicians in formulating differentiated treatment strategies for specific patient subtypes, thereby optimizing therapeutic outcomes and prognosis.

Materials and methods

Data source

This study analyzed low-dose chest CT images from 289 patients with histopathologically confirmed lung adenocarcinoma. The cohort comprised 172 cases of MIA, 50 cases of IAC, and 67 cases of AIS. All patients underwent low-dose chest CT scans using two systems: the United Imaging 760 CT (42–126 mA, 120 kV, 1 mm slice thickness, matrix 512×512) and the Siemens Emotion 16 CT (34–123 mA, 130 kV, 1 mm), both employing standard reconstruction algorithms and conventional low-dose modes. Baseline demographic and clinical variables included sex, age, smoking history, and pathological grade (**Table 1**).

The dataset comprised CT images from 289 patients, capturing multi-slice imaging features with continuous lesion layers. Lesions were initially segmented by radiologists, who placed seed points at the lesion centers. Subsequently, a region-growing algorithm was applied to automatically delineate three-dimensional lesion boundaries, and radiomics feature were extracted using specialized software. This process

Table 2. Selected radiomic features and their meanings

Raw Feature	Feature Meanings
Original_shape2D_PixelSurface	2D pixel surface shape feature of the original image.
Square_gldm_DependenceNonUniformity	Dependence nonuniformity derived from the gray level dependence matrix of the square-shaped image.
Original_firstorder_Energy	First-order energy feature of the original image.
Original_shape2D_MinorAxisLength	2D minor axis length shape feature of the original image.
Wavelet-LL_gldm_SmallDependenceHighGrayLevelEmphasis	Small dependence high gray level emphasis derived from the gray level dependence matrix of the LL sub-band of the wavelet-transformed image.
Original_firstorder_RobustMeanAbsoluteDeviation	First-order robust mean absolute deviation feature of the original image.
Wavelet-LL_firstorder_RobustMeanAbsoluteDeviation	First-order robust mean absolute deviation feature of the LL sub-band of the wavelet-transformed image.
Square_firstorder_InterquartileRange	First-order interquartile range feature of the square-shaped image.
Original_shape2D_MeshSurface	2D mesh surface shape feature of the original image.
Original_gldm_SmallDependenceHighGrayLevelEmphasis	Small dependence high gray level emphasis derived from the gray level dependence matrix of the original image.
Logarithm_glcm_Idn	Inverse Difference Normalized (Idn) derived from the gray level co-occurrence matrix of the logarithmic image.
Gradient_glrlm_ShortRunLowGrayLevelEmphasis	Short run low gray level emphasis derived from the gray level run length matrix of the gradient image.

yielded 963 radiomics features, including spatial relationships, morphological characteristics, density, and higher-order texture descriptors. Among these, 11 were categorical variables, while 952 were continuous. As the categorical features primarily described spatial and morphological characteristics with limited predictive relevance, subsequent feature processing focused on screening and dimensionality reduction of the continuous variables. High-contrast features were selected for model training to enhance objectivity and reproducibility.

Feature extraction

During the feature extraction phase, analysis of variance-was initially applied to screen variables. Columns with a variance<1 were removed to eliminate features contributing minimally to the results, leaving 515 continuous variables. Using the corr() function in Python for correlation analysis, we quantified inter-variable relationships and identified highly correlated or weakly informative features, reducing the dataset to 194 variables. Subsequently, the tsfresh package was used to generate time-series–based descriptors. The 1,667×194 feature matrix was processed with the extract_features algorithm and partitioned into 289 groups based on “group” and “group_id” columns. For each group of 194 variables, we derived maxima, autocorrelation, and other features, forming a new dataset of 289×150,336 dimensions. Subsequently, the select_features function was then applied to assess feature relevance and remove uninformative variables, retaining approximately 5% of features and producing a reduced dataset of 289×79,220.

Finally, a random forest algorithm was employed for feature ranking and optimization. Feature importance scores were computed with respect to the target outcome, enabling the identification of highly predictive variables. The top 15 most important features were selected and mapped back to the original dataset, forming the final optimized feature subset (**Table 2**).

Model architecture

A classification model was constructed based on the multi-head attention mechanism and Transformer network (**Figure 2**). Within this framework, multiple self-attention units were integrated, and their outputs were concatenated, enabling efficient parallel training.

By combining multi-head attention with position-wise feed-forward networks, the Transformer eliminated the need for additional convolutional or recurrent layers, simplifying the architecture while enhancing parallel computing efficiency without compromising model performance [18]. The parameters of the model are detailed in **Table 3**.

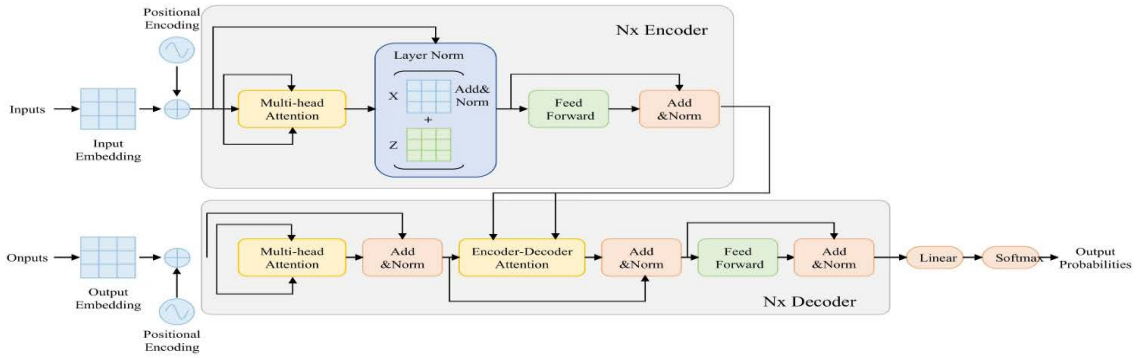

Figure 2. Multiple attention mechanisms and Transformer model diagrams.

Table 3. Model parameters and their specifications

Parameter	Description	Value
NUM_head	Number of heads in the multi-head attention mechanism	6
Dropout	Dropout rate to prevent overfitting	0.1
Hidden	Dimension of the hidden layer	512
LR	Learning rate (controls the update speed of parameters during training)	1e-3
Vocab_size	Vocabulary size	15
Embed_dim	Embedding dimension of the feature vectors	120
Epoch	Number of training epochs	150
Batch_size	Mini-batch size for training	64

The proposed model adopts an encoder-decoder architecture. The encoder integrates multi-head self-attention and position-wise feed-forward layers to extract high-dimensional dependencies from the input features. The decoder further refines these representations by incorporating encoder-decoder attention and projecting the output through a softmax classifier. Positional encoding helps preserve the sequential nature of radiomic data. This architecture effectively captures long-range dependencies and complex feature relationships derived from CT images, thereby supporting accurate subtype classification.

Assessment indicators

To comprehensively evaluate the segmentation performance of the model, the following key evaluation metrics were employed:

Accuracy

Accuracy reflects the proportion of predictions correctly classified by the model. It integrates true positives (TP), true negatives (TN), false positives (FP), and false negatives (FN), thus indicating whether the overall predictions are correct. In lung adenocarcinoma subtype classification, higher accuracy indicates that the model correctly identifies a larger proportion of cases. The calculation formula is as follows:

$$\text{Accuracy}=\frac{1}{N}\sum_{i=1}^{N}\frac{(TP+TN)_i}{(TP+FP+TN+FN)_i} \quad (1)$$

Recall

Recall represents the proportion of samples belonging to a given positive class that are correctly identified by the model. In the deep learning-driven three-class classification of lung adenocarcinoma, when any subtype is designated as the positive class, a high recall indicates that the model can effectively capture its pathological features, thus reducing the risk of underdiagnosis. The formula is as follows:

$$\text{Recall}=\frac{1}{N}\sum_{i=1}^{N}\frac{(TP)_i}{(TP+FN)_i} \quad (2)$$

F1-Score

The F1-score is the harmonic mean of precision and recall. Since precision and recall may trade off against each other, relying on a single indicator may not fully reflect model performance. The F1-score integrates both measures, and a higher value indicates that the model achieves a better balance between precision and recall,

Table 4. Performance metrics of the Transformer model

	Accuracy	F1-score	Recall	AUC
Training	0.980	0.942	0.940	0.990
Validation	0.914	0.874	0.871	0.880

Note: AUC, area under the curve.

thereby providing a more comprehensive assessment of its ability to classify lung adenocarcinoma subtypes. The calculation formula is as follows:

$$\text{F1-score}=2\times\frac{\text{Precision}\times\text{Recall}}{\text{Precision}+\text{Recall}} \quad (3)$$

Area under the curve (AUC)

AUC refers to the area under the receiver operating characteristic curve, which plots the false positive rate (FPR) on the x-axis and the true positive rate (TPR) on the y-axis. The FPR and TPR are defined as:

$$\text{FPR}=\frac{\text{FP}}{\text{FP}+\text{TN}} \quad (4)$$

$$\text{TPR}=\frac{\text{TP}}{\text{TP}+\text{FN}} \quad (5)$$

AUC values range from 0.5 to 1.0, with larger values indicating a stronger ability to discriminate between classes. In the classification of lung adenocarcinoma subtypes, a higher AUC value indicates that the model can more effectively distinguish among the three lung adenocarcinoma subtypes.

Results

The performance metrics of the Transformer model, including accuracy (training_accuracy and val_accuracy), F1-score, recall, and AUC, are detailed in **Table 4**.

Figure 3A depicts the accuracy curves for the training and validation sets over 150 epochs, clearly illustrating the progression of model accuracy. Accuracy typically increases as training proceeds, eventually approaching a plateau. As expected, the training accuracy remains consistently higher than the validation accuracy.

Figure 3B illustrates the loss variation curve per epoch during Transformer model training. This curve tracks loss values at each epoch or batch during the training process, serving as a key metric for monitoring model performance and fine-tuning hyperparameters. In the initial phase, losses typically decrease as training iterations progress, demonstrating the model's gradual acquisition of more features and patterns. Subsequently, losses may plateau or fluctuate when the model reaches local optima and achieves optimal data fitting. If losses start to increase, this indicates either overfitting the training data or improper hyperparameter configuration.

In this study, **Figure 3C** and **Figure 3D** demonstrate the classification performance of the Transformer model across training and test datasets, as assessed by receiver operating characteristic curves and their AUC values. The receiver operating characteristic curve serves as a crucial metric for assessing model classification accuracy, and its AUC provides a comprehensive measure of model performance across various thresholds.

A higher AUC indicates stronger discriminative capability, while appropriate adjustment of the decision threshold can balance TPR and FPR, thereby improving prediction precision. The Transformer model achieved an AUC of 0.990 on the training set, demonstrating exceptional classification accuracy and strong learning capacity. On the validation set, the AUC reached 0.880-slightly lower but still indicative of satisfactory generalization to unseen data.

Overall, the Transformer model exhibited superior classification performance across both datasets, establishing a solid foundation for future research and clinical applications. Future studies could further investigate the impact of different threshold settings to optimize the model's classification effectiveness.

The Transformer model achieved a classification accuracy of 0.980 in the training set and 0.914 in the validation set. The corresponding recall rates were 0.942 and 0.874, F1-scores were 0.940 and 0.871, and AUC values were 0.990 and 0.880, respectively. Meanwhile, the loss function approached zero, indicating stable convergence. These findings demonstrate that the model combining multi-head attention and Transformer architecture delivers robust performance in classifying lung adenocarcinoma

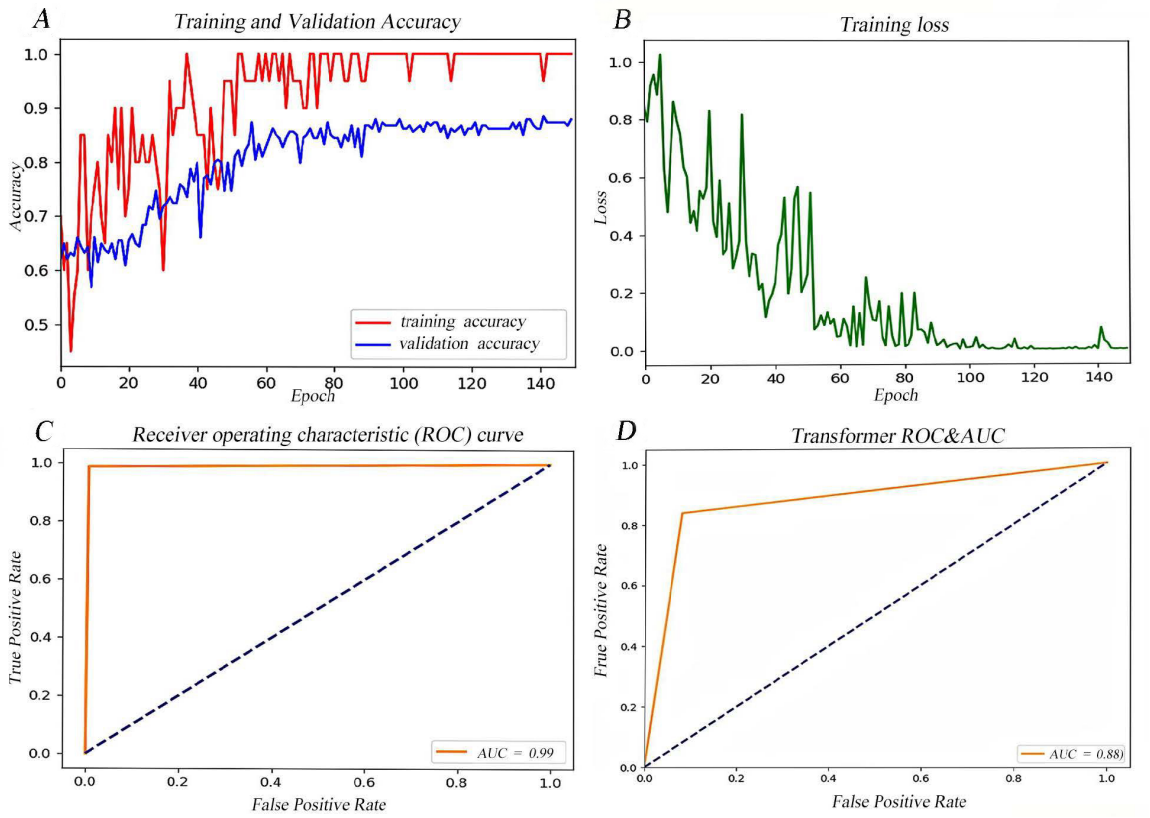

Figure 3. Performance evaluation of the Transformer model in training and validation sets. (A) Accuracy curves of training and validation sets across 150 epochs, showing steady improvement and convergence; (B) Training loss curve, indicating rapid reduction and stabilization with minimal overfitting; (C) ROC curve of the training set, demonstrating high classification capability with an AUC of 0.99; (D) ROC curve of the validation set, indicating good generalization with an AUC of 0.88. ROC, receiver operating characteristic; AUC, area under the curve.

subtypes from CT images. Moreover, the results suggest that variations in radiological features captured by CT imaging can effectively reflect lesion types, highlighting the model's potential as a valuable auxiliary diagnostic tool.

Discussion

This study presents a Transformer-based model incorporating multi-head self-attention mechanisms for classifying the three major subtypes of lung adenocarcinoma. By integrating radiomics and imaging features, the model achieved excellent performance on the training and validation sets, demonstrating high accuracy and robustness in lung adenocarcinoma subtype classification.

Previous research has reported encouraging results using deep learning for similar tasks. Ma et al. developed a deep learning model for predicting lymph node metastasis in lung adenocarcinoma, achieving AUC values of 0.948 and 0.961 in the training and validation sets, respectively [19]. Additionally, Liu et al. proposed an image-omics-based multi-subtype classification model for non-small cell lung cancer, achieving an accuracy of approximately 0.860 [20]. Although these studies highlight the potential of traditional methods and early-stage deep learning approaches, further optimization remains possible. The Transformer model introduced in this study effectively captures global contextual information and long-range dependencies, which is particularly important for identifying complex subtypes of lung adenocarcinoma. Furthermore, the multi-head self-attention mechanism enables the model to analyze feature relationships from multiple perspectives, enabling more precise differentiation among subtypes. This innovative approach demonstrates clear advantages in processing high-dimensional radiomic data, resulting in superior model performance compared to previous studies.

This study also has several limitations. First, the relatively small dataset may affect feature extraction and parameter optimization during radiological classification. Additionally, insufficient training samples are a critical issue, since high-quality predictive models require adequate data to prevent overfitting, particularly for deep learning architectures like Transformer net-

works, which typically demand massive training datasets. Thus, sample scarcity remains a key constraint on prediction accuracy. Second, the current approach relies exclusively on CT imaging for radiological feature extraction, which may compromise disease analysis precision due to limited diagnostic scope. While the model effectively classifies lesions through pattern recognition, feature selection variations could introduce bias. Furthermore, while trend analysis demonstrates potential for lesion identification, its limited applicability in clinical decision support, rule discovery, and interpretability may compromise diagnostic reliability. Collectively, these factors may reduce model accuracy and limit its effectiveness as an auxiliary diagnostic tool.

Clinical interpretability and practical significance

The radiomics model developed in this study not only achieves accurate classification of lung adenocarcinoma subtypes (AIS, MIA, IAC) but also demonstrates good clinical interpretability. In clinical practice, this model is designed to function as an auxiliary tool for radiologists rather than a replacement. By leveraging radiomics-derived risk scores and subtype predictions, radiologists can obtain quantitative information regarding lesion spatial structure, morphological features, density variations, and texture patterns, thereby enhancing their routine CT image evaluations.

By integrating the model's feature-importance rankings with imaging characteristics, physicians can more intuitively identify which radiological features most effectively distinguish pathological subtypes. For instance, higher-order texture features may indicate intra-tumor heterogeneity, while morphological parameters can reflect tumor margin infiltration. Such quantitative insights facilitate comprehensive decision-making in surgical planning, lesion grading, and follow-up strategy formulation. Furthermore, collaboration between AI models and clinicians enhances diagnostic efficiency. Physicians can utilize these models to rapidly screen suspected subtypes and verify the predictions using their expertise, fostering an "AI-assisted, physician-guided" diagnostic workflow. This approach promotes evidence-based decision-making while mitigating the risks of misdiagnosis associated with over-reliance on AI systems.

Future work

Future research will focus on addressing the current limitations of this study. In terms of data and sample size, we will expand the dataset through multi-institutional collaborations and apply data augmentation techniques to enrich training samples. These strategies will provide the model with a broader and more diverse learning foundation to effectively mitigate overfitting.

For image selection, we plan to incorporate multimodal imaging techniques such as MRI and X-ray for joint analysis, capturing lesion characteristics from multiple perspectives and improving diagnostic accuracy. Regarding feature selection, we will optimize screening algorithms and integrate clinical prior knowledge to enhance the effectiveness of feature-trend analysis in lesion identification, reducing the impact of feature variations on classification results. Additionally, we will prioritize improving the model's utility in clinical decision support by enhancing interpretability and mining decision rules, allowing the system to better assist radiologists and enhance its applicability in routine practice.

As an emerging classification method, multidimensional lesion feature analysis based on recurrent networks enhances prediction accuracy by integrating clinical and imaging features, thereby facilitating early cancer detection and precision therapy. This approach is poised for expanded applications in medicine, bioinformatics, computer vision, and related fields. With technological advancements, more efficient automated classification methods are expected to drive breakthroughs in disease diagnosis and therapeutic innovation.

Conclusion

This study developed a Transformer-based deep learning framework for classifying lung adenocarcinoma subtypes (MIA, AIS, IAC). The framework enhances sequence feature learning capabilities through multi-head attention mechanisms and fully connected layers, thereby improving model generalization and reducing overfitting. This approach enables effective training and accurate classification of radiomics features.

Experimental results demonstrate that the proposed Transformer model, integrating CT-derived radiomics features, exhibits superior performance in classifying lung adenocarcinoma subtypes. These findings validate both the diagnostic capabilities of imaging features and the clinical utility of the model. Meanwhile, radiomics provide diagnostic support from multidimensional perspectives, including morphology and

grayscale, while the sequential analysis of feature variations offers greater diagnostic value than isolated features, providing new insights for incorporating radiological characteristics into clinical decision-making.

Author contributions: Linrong Yuan, Yutong Xie, and Danhong Li jointly designed the study, developed the Transformer-based classification model, and drafted the manuscript. Jianghui Li, Miao Yu, Siqi Wang and Yu Wang were responsible for CT image preprocessing, radiomic feature extraction, model training, and performance evaluation. He Ren supervised the project, provided critical revisions, and approved the final version of the manuscript.

References

[1] Chen W, Zhang S, Zou X. Zhongguo Fei Ai Za Zhi 2010;13(5):488-493.

[2] Han B, Zheng R, Zeng H, et al. Cancer incidence and mortality in China, 2022. J Natl Cancer Cent 2024;4 (1):47-53.

[3] Li H, Zhao M, Fei G, et al. Epidemiological trends and incidence prediction of lung cancer in China based on the Global Burden of Disease study 2019. Front Med (Lausanne) 2022;9:969487.

[4] Guo L, Zhu C, Cai L, et al. Global burden of lung cancer in 2022 and projected burden in 2050. Chin Med J (Engl) 2024;137 (21):2577-2582.

[5] Li X, Zhang W, Yu Y, et al. CT features and quantitative analysis of subsolid nodule lung adenocarcinoma for pathological classification prediction. BMC Cancer 2020;20(1):60.

[6] Chen H, Carrot-Zhang J, Zhao Y, et al. Genomic and immune profiling of pre-invasive lung adenocarcinoma. Nat Commun 2019;10(1):5472.

[7] Su H, Chen L, Wu J, et al. Proteogenomic characterization reveals tumorigenesis and progression of lung cancer manifested as subsolid nodules. Nat Commun 2025;16(1):2414.

[8] Wu Z, Zhao Y, Peng Y, et al. LncRNA TMEM99 Complexes with IGF2BP2 to Inhibit Autophagy in Lung Adenocarcinoma. Adv Sci (Weinh) 2025;12(33):e202507871.

[9] Wang J, Lin L, Zhao S, et al. Sheng Wu Yi Xue Gong Cheng Xue Za Zhi 2019;36(4):670-676.

[10] Zhou J, Hu B, Feng W, et al. An ensemble deep learning model for risk stratification of invasive lung adenocarcinoma using thin-slice CT. NPJ Digit Med 2023;6(1):119.

[11] Shuvo S, Mamun TB. AutoLungDx: A Hybrid Deep Learning Approach for Early Lung Cancer Diagnosis Using 3D Res-U-Net, YOLOv5, and Vision Transformers. 2023.

[12] Yu P, Zhang H, Wang D, et al. Spatial resolution enhancement using deep learning improves chest disease diagnosis based on thick slice CT. npj Digit Med 2024;7(1):335.

[13] Kuang H, Wang Y, Liu J, et al. Hybrid CNN-Transformer Network With Circular Feature Interaction for Acute Ischemic Stroke Lesion Segmentation on Non-Contrast CT Scans. IEEE Trans Med Imaging 2024;43(6):2303-2316.

[14] Azad B, Adibfar P, Fu K. TransDAE: Dual Attention Mechanism in a Hierarchical Transformer for Efficient Medical Image Segmentation. arXiv arXiv:2409.02018, 2024.

[15] Zhang Y, Xi R, Wang W, et al. Low-Contrast Medical Image Segmentation via Transformer and Boundary Perception. IEEE Trans Emerg Top Comput Intell 2024;8(3):2297-2309.

[16] Jing R, Wang J, Li J, et al. A wavelet features derived radiomics nomogram for prediction of malignant and benign early-stage lung nodules. Sci Rep 2021;11(1):22330.

[17] Hussein S, Gillies R, Cao K, et al. TumorNet: Lung nodule characterization using multi-view Convolutional Neural Network with Gaussian Process. 2017 IEEE 14th International Symposium on Biomedical Imaging (ISBI 2017) 2017;1007-1010.

[18] Papagiannopoulou A, Angeli C. Social Media Text Summarization: A Survey Towards a Transformer - based System Design. Adva Sci, Technol Eng Syst J 2023;8(6):26-36.

[19] Ma X, Xia L, Chen J, et al. Development and validation of a deep learning signature for predicting lymph node metastasis in lung adenocarcinoma: comparison with radiomics signature and clinical - semantic model. Eur Radiol 2023;33(3):1949-1962.

[20] Liu J, Cui J, Liu F, et al. Multi-subtype classification model for non-small cell lung cancer based on radiomics: SLS model. Med Phys 2019;46(7):3091-3100.